Limit Cycle Analysis Applied to the Oscillations of Decelerating Blunt-Body Entry Vehicles

Mark Schoenenberger and
Dr. Eric M. Queen
NASA Langley Research Center
Hampton, VA 23681

ABSTRACT

Many blunt-body entry vehicles have nonlinear dynamic stability characteristics that produce self-limiting oscillations in flight. Several different test techniques can be used to extract dynamic aerodynamic coefficients to predict this oscillatory behavior for planetary entry mission design and analysis. Most of these test techniques impose boundary conditions that alter the oscillatory behavior from that seen in flight. Three sets of test conditions, representing three commonly used test techniques, are presented to highlight these effects. Analytical solutions to the constant-coefficient planar equations-of-motion for each case are developed to show how the same blunt body behaves differently depending on the imposed test conditions. The energy equation is applied to further illustrate the governing dynamics. Then, the mean value theorem is applied to the energy rate equation to find the effective damping for an example blunt body with nonlinear, self-limiting dynamic characteristics. This approach is used to predict constant-energy oscillatory behavior and the equilibrium oscillation amplitudes for the various test conditions. These predictions are verified with planar simulations. The analysis presented provides an overview of dynamic stability test techniques and illustrates the effects of dynamic stability, static aerodynamics and test conditions on observed dynamic motions. It is proposed that these effects may be leveraged to develop new test techniques and refine test matrices in future tests to better define the nonlineary functional forms of blunt body dynamic stability curves.

NOMENCLATURE

A	Angle-of-attack constant	R	Earth radius
C_A	Axial force coefficient	S	Reference area
C_D	Drag force coefficient	T	Period of oscillation
C_L	Lift force coefficient	t	Time
C_{L_α}	Lift-curve slope	V	Velocity
$\overline{C_{L_\alpha} + C_{m_q}}$	Effective damping with lift effects	Greek	
C_{m_α}	Pitching moment slope	α	Angle-of-attack
$C_{m_q} + C_{m_{\dot\alpha}}$	Pitch damping coefficient	γ	Flight-path angle
$\overline{C_{m_q}}$	Effective pitch damping	δ	Phase shift constant
C_N	Normal force coefficient	μ	Euler-Cauchy damping constant
d	Reference diameter	ν	Euler-Cauchy frequency constant
f	Unspecified function	$\xi_{1,2}$	Constant velocity damping coeffs.
g	Gravitational acceleration	ρ	Density
I	Moment-of-inertia	ω	Oscillation frequency
K	Oscillatory energy	Subscripts	
M	Mach	i, f	Initial and final conditions
m	Mass	0	Function of oscillation amplitude

1.0 INTRODUCTION

Blunt bodies have been used for decades to protect and decelerate robotic payloads through atmospheres on other planets and to safely return human and robotic payloads to earth. Various sphere-cone and spherical-section forebodies have proven to be efficient designs for decelerating payloads and astronauts from very large entry speeds, while minimizing the peak heating and heat load the vehicle must withstand. However, one well-documented, adverse aerodynamic property associated with many blunt vehicles is a bounded dynamic instability that tends to start near Mach 3.5, becoming more unstable with decreasing Mach number. These instability can cause blunt-body oscillations to grow so much that a safe parachute deployment is not possible. In extreme cases, dynamic instability can result in a capsule tumbling if not assisted by a drogue parachute or other stabilizing device.

The pitch damping characteristics of blunt bodies tend to be nonlinear. For non-lifting vehicles (e.g. axisymmetric with no radial cg offset) the peak pitch damping coefficient (most unstable) occurs at $\alpha = 0°$, dropping off and becoming negative at larger angles-of-attack. For constant velocity flight, a statically stable blunt body oscillates and reaches equilibrium at a limit cycle where undamping dynamic moments are balanced by the damping moments at large angles-of-attack. This is true for full-scale vehicles and also occurs during ground-based ballistic range testing. As the vehicle decelerates, dynamic pressure drops and static pitching moments on the vehicle are reduced. This relaxation of the static stability "spring stiffness" causes a decrease in frequency and increase in oscillation amplitude. Therefore a blunt body reaching an oscillation amplitude equilibrium in a constant velocity flight will exhibit amplitude growth in decelerating flight.

Forebody shapes are typically driven by heating and static stability constraints. Packaging and mass requirements tend to drive the backshell shapes. Therefore backshell geometries are as varied as the missions for which they are used. The backshell geometry is thought to be the dominant factor effecting how the wake structure interacts with the body and ultimately the level of dynamic stability of the vehicle. There are ongoing efforts to predict blunt-body dynamic stability using computational methods [1, 2], but to date, no practical

predictive capability exists. Experimental methods remain a fundamental component in the assessment of blunt body dynamic stability. Ballistic range testing is a frequently used technique. Free flight data in a ballistic range is not corrupted by a sting disrupting the wake flow. Also, when properly scaled, the flight dynamics are essentially the same as seen in a full-scale flight, whereas wind tunnels are typically limited to oscillations about a fixed point. One exception is a vertical spin tunnel, where the capsule is again flying freely with the weight of the model in equilibrium with the drag acting upon it. The flight-like motions achieved in the ballistic range or spin tunnel has advantages and disadvantages. While these techniques give a good representation of the motions expected in flight, the dynamic moments driving the motions are difficult to quantify in coefficient form for use in simulation, as no direct measurement of the forces and moments acting on the vehicle are possible.

The nonlinear characteristics of blunt body dynamics, and the difficulty in modeling the governing flow physics, coupled with the amplitude changes due to deceleration combine to obfuscate the interchange of forces and moments on the capsule as it moves along a trajectory. Limit-cycle analysis helps explicate the nonlinear pitch damping characteristics of blunt capsules, but velocity changes make limit-cycle analysis more complicated. This work attempts to separate the capsule aerodynamic characteristics from the trajectory effects and from test conditions to interpret ballistic range results and the role of dynamic stability in the overall stability of a blunt capsule in flight. The effects of dynamic stability on oscillations in three scenarios are provided: constant velocity, free-to-oscillate; constant velocity, free-to-heave and oscillate; and decelerating, free-to-heave and oscillate. The oscillation energy equation and analytic solutions are used to show how pitch damping characteristics, the lift-curve slope and other factors influence the flight dynamics in these scenarios .

The goal of this paper is to provide an overview of blunt body flight characteristics for those new to blunt body aerodynamics and demonstrate the effects of different test conditions on the observed dynamics. Others have looked at blunt body limit cycles in some detail. For example, Chapman and Yates [3] give an excellent explanation of limit cycle analysis as applied to blunt body aerodynamics. The work presented here uses simplified equations of motion to identify and compare the first-order effects on blunt body dynamics. Analytic solutions and numerical simulations are used to illustrate to those new to dynamic instabilities and aerodynamic limit cycles, the contributions of dynamic and static aerodynamics and freestream conditions to the oscillatory behavior of blunt bodies and the addition or removal of oscillatory energy. Even among aerospace engineers who work with entry capsules, the interplay of linear capsule motion, unsteady aerodynamic forces and oscillatory motion is not always appreciated at a fundamental level. This paper attempts to provide a framework to help the engineer understand the roles of different forces and moments acting on a blunt body that result in limit-cycle or near limit-cycle motions.

2.0 TEST TECHNIQUES AND APPLICATIONS

To understand the examples presented in later sections, a brief overview of different dynamic aerodynamic test techniques is presented. There are several techniques commonly used. Within each type are variations which can effect the observed capsule motions. Each technique has benefits and limitations. Variations of two major types of testing are described and then contrasted with planetary entry trajectories. From these different test techniques, three cases will be used for comparison by analytic solution in the following section. The cases are then assessed in terms of the oscillatory energy and the mechanisms by which energy enters and departs the system. A discussion of limit cycles is then presented for each of the three cases.

2.1 Dynamic Wind Tunnel Testing

Wind tunnel tests techniques [4, 5] are perhaps the oldest and best documented ways of measuring dynamic aerodynamic coefficients. Fundamentally, the techniques are the same as static wind tunnel testing with models being held in a tunnel as the freestream flow passes over the model. Additionally, dynamic testing imposes model motion, or frees the model to respond dynamically on its own, relative to the freestream flow. This model motion is typically oscillatory. Extra forces and moments act upon the model due to these oscillations, beyond the forces and moments measured in a static test. The dynamic aerodynamic coefficients are recorded as the derivatives of the additional forces and moments introduced by the dynamic motions with respect to the rates at which the model was moving as the data was recorded.

Free-to-Oscillate

In free-to-oscillate testing, a model is held in a wind tunnel on a sting at a fixed position like traditional static wind tunnel testing. However, the sting also permits oscillatory motion of the model with either bearings or a spring. The model is perturbed from its equilibrium position and the model oscillates freely, either damping down or growing, based on the dynamic stability inherent in the model geometry. Figure 1 shows a typical free-to-oscillate test setup as was used for the Apollo command module.

Free-to-oscillate testing is very simple to perform and can be modeled very easily for parameter identification. However, it can be difficult to achieve meaningful results. Precise measurement of the capsule position versus time is required, and bearing friction and the presence of a sting can affect the motion of the model, masking the true dynamic behavior. After data is acquired, parameter identification techniques are applied to the model motion history to extract aerodynamic coefficients. A wind tunnel setup is generally a more controlled environment than free flight, potentially producing more repeatable results, with greater control over initial conditions. However, this technique is still limited by not having any direct moment measurements. In that way, the free-to-oscillate technique is similar to ballistic range testing.

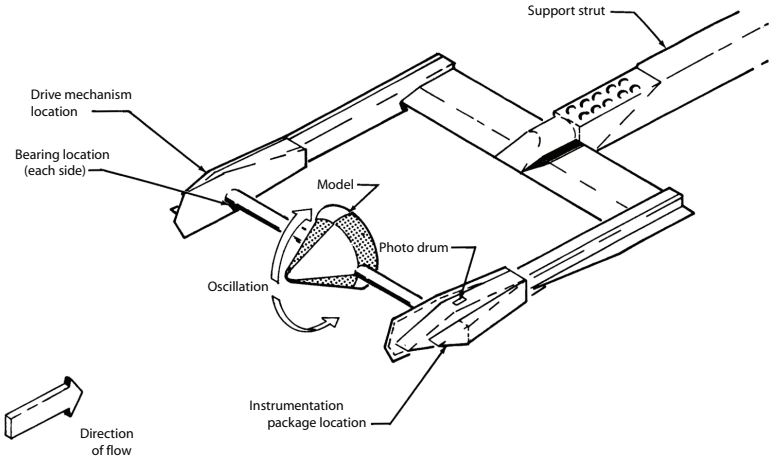

Figure 1: Free-to-oscillate setup[6]

Spin Tunnel

In a vertical spin tunnel the freestream flow is directed vertically upward with the model perpetually "falling" relative to the flow. These facilities are commonly used to measure the terminal-velocity dynamics of blunt bodies at low speeds [6]. Often, the models are dynamically scaled, achieving dynamics very similar to those at flight conditions. Figure 2 shows a cross section of the NASA Langley 20 Foot Spin Tunnel and a test photograph from the Mercury program [7, 8]. In a spin tunnel, the drag acting on the model is balanced by its weight. Angle-of-attack oscillations of the model can cause the drag force to fluctuate which then causes a vertical motion relative to the oncoming flow (and test section). For large changes in drag, control of the freestream velocity may be required to keep the model within the test section. For small oscillations, drag is nearly constant and this test technique achieves constant velocity conditions with the model free to oscillate and heave. Heaving motion is a periodic translation caused by the lift produced as the model oscillates in angle-of-attack. This translational motion results in a flight path angle oscillation about the mean ($\gamma_{mean} = 90°$). It will be shown that this additional freedom of movement results in a change in the effective damping as compared to free-to-oscillate testing where the model is held on a sting.

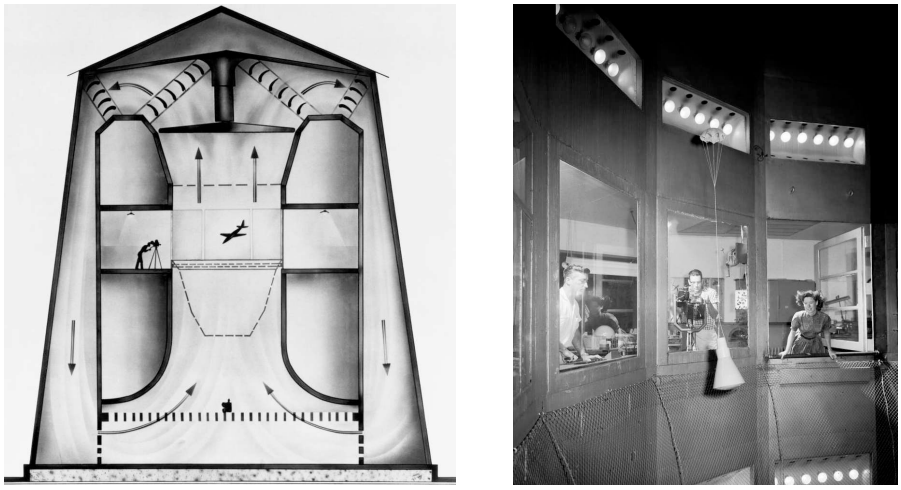

(a) Cross Section of Tunnel

(b) Mercury Capsule with Drogue Parachute

Figure 2: NASA Langley 20 Foot Spin Tunnel

Forced Oscillation

Forced-oscillation testing is very similar to free-to-oscillate testing, but instead of the model rotating freely, it is forced through prescribed oscillatory motions and the damping can be determined explicitly [4, 5, 9]. Forced oscillation techniques have excellent control over all the important test parameters. The model motion is driven by a motor, so it is possible to test a wide range of amplitudes and frequencies without requiring complicated and the sometimes geometry-limiting need to scale the model mass properties. Forced oscillation testing directly measures the forces and moments acting on the vehicle and damping coefficients can be directly calculated from those force and moment measurements. As the motions are prescribed, this is not a method conducive to observing limit-cycle oscillations. The data measured with this testing may be more accurate than other methods and can be used to predict limit cycle oscillations in flight. However, the controlled nature of the

testing prevents this technique from being compared in this work.

2.2 Ballistic Range Testing

Ballistic range testing is essentially a scaled flight test [10–12]. Ranges can be an indoor facility or an outdoor range, where the models are tracked with radar. In an indoor range, models fly freely down an instrumented range, producing flight-like motions from which aerodynamic coefficients are extracted. The models are launched from a gun, held at an initial orientation by a sabot. The gun propels the model to the desired initial velocity and upon exiting the gun barrel, the sabot petals peel away leaving the model to fly down the instrumented portion of the range. The sabot petals are arrested so as not to interfere with downrange measurements. Orthogonal shadowgraphs are taken at multiple stations down the range. Calibrated reference points in the images enable the model position and orientation to be determined at each station. As the spark source, illuminating the shadowgraphs is triggered at each station, the time is recorded with a chronograph. Figure 3 shows an example of this setup in the Eglin Air Force Base (AFB) Aeroballistic Research Facility (ARF). The geometry used to identify the capsule position and orientation from shadowgraphs is illustrated for one station in the range.

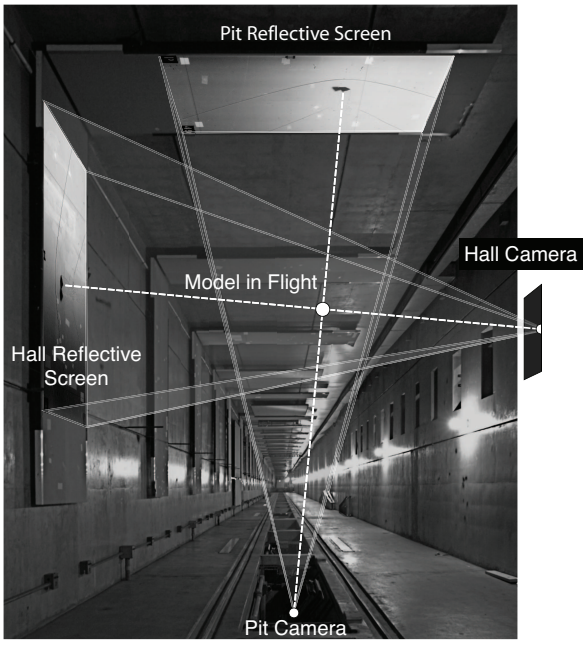

Figure 3: Looking up-range at the Eglin AFB Aeroballistic Research Facility

The time, position and orientation of the model at each station is then used to reconstruct the full trajectory. Parameter identification techniques are then used to extract aerodynamic coefficients from the observed trajectories. Multiple shots with different initial oscillation amplitudes and velocities help identify the aerodynamics over a range of angles-of-attack and Mach number. More data helps to more accurately define the functional form of nonlinear aerodynamic coefficients and reduce uncertainties.

For outdoor testing a gun is again used to launch the model. Instrumentation onboard the capsule measures the body rotations and sensed accelerations, while radar tracks the models in flight for independent measurements of position and velocity. The onboard and radar measurements are used to reconstruct the model tra-

jectory, very much like a full scale entry vehicle. Parameter identification techniques are then used to extract aerodynamics much like what is done for indoor testing. An outdoor range permits the testing of lifting vehicles, that would strike the walls of an indoor range. However, as models are not typically recoverable, the costs to instrument each shot can be prohibitive.

While this technique has the overwhelming benefit of achieving flight-like motions, there are several drawbacks and limitations. Chief among them, this test technique does not allow a direct measurement of aerodynamic coefficients. While multiple fits through the data points of many trajectories are done together to find the best fit for the aerodynamic coefficients, the problem is still under-defined. Different functional forms can achieve very similar fits through the data points. This is especially true for the pitch and yaw damping coefficients which tend to be very nonlinear with angle-of-attack and Mach number. Having a good understanding of the relative contributions to capsule motion from drag, lift and damping terms, as well as the effects of mass properties and freestream conditions can be very useful in interpreting the observed motions and can assist in parameter identification efforts.

2.3 Planetary Entry

All ground-based data is gathered for the purpose of predicting flight performance. A planetary entry capsule experiences flight conditions that change even more dramatically than those seen by a ballistic range model. While decelerating, the capsule sees increasing, then decreasing dynamic pressure as the freestream density and pressure increase along the capsule's descent. Depending on the vehicle mass properties and freestream conditions, the change in flight path angle due to gravity can also affect the capsule dynamics. These more complex effects are beyond the scope of this work, but pointed out to emphasize that first understanding the mechanisms at play in different ground-based test methods is important to interpreting observed oscillatory motions and the extracted dynamic data and predicting how those motions will change in flight.

3.0 EQUATIONS OF MOTION

The planar equations of motion for a body flying in a gravity field is a good place to start for the motions in planetary entry and can be simplified to describe all of the motions achieved in ground based testing. The planar motions are described by Equations 1 through 3. Equation 1 describes the sum of the forces acting on the body in the direction of motion. Equation 2 describes the change in flight path angle, γ, due to forces normal to the direction of motion, gravity and centrifugal forces as the body curves around a planet. Equation 3 sums the inertial, static and dynamic moments acting on the vehicle. These equations are valid for a low lift-to-drag vehicle at small angles-of-attack (α approximately less than 30° for these shapes). Unless otherwise noted, the analysis in this paper assumes that lift and pitching moment vary linearly with angle-of-attack, drag is invariant with angle-of-attack and all aerodynamic coefficients are invariant with velocity/Mach number. The coordinate system for these Equations is shown in Figure 4.

$$\dot{V} = -\frac{\rho V^2 S C_D}{2m} - g \sin\gamma_o \tag{1}$$

$$\dot{\gamma} = \frac{\rho V S C_L}{2m} - \left(\frac{g}{V} - \frac{V}{R}\right)\cos\gamma_o \tag{2}$$

$$\ddot{\theta} = \frac{\rho V^2 S d}{2I}\left(C_{m_q}\frac{\dot{\theta}d}{2V} + C_{m_{\dot{\alpha}}}\frac{\dot{\alpha}d}{2V} + C_{m_\alpha}\alpha\right) \tag{3}$$

Where

$$\theta = \alpha + \gamma \tag{4}$$

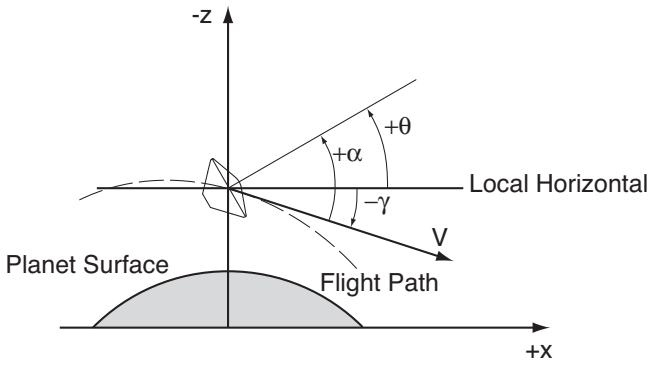

Figure 4: Coordinate system

Some simplifying assumptions may be made that permit the moment equation be cast as a differential equation that can be solved analytically. First, it is assumed that gravity and centrifugal effects are small, meaning the mean flight path angle over a trajectory segment is effectively constant. These assumptions simplify the RHS of Equation 2 to just the contribution due to lift. Flight path angle varying due to lift only is a valid assumption for many ballistic range flights, spin tunnel flight and some free-to-oscillate wind tunnel test conditions. It is also assumed that lift and pitching moment vary linearly with angle-of-attack. With those assumptions, Equation 4, and its first and second derivatives can be used with Equations 1 and 2 to express Equation 3 in terms of angle-of-attack only. First, the LHS becomes

$$\ddot{\alpha} + \left(\frac{\rho V S}{2m}\right)^2 C_D C_{L_\alpha} \alpha + \frac{\rho V S}{2m} C_{L_\alpha} \dot{\alpha} = \frac{\rho V^2 S d}{2I} \left(C_{m_q} \frac{\dot{\theta} d}{2V} + C_{m_{\dot{\alpha}}} \frac{\dot{\alpha} d}{2V} + C_{m_\alpha} \alpha \right) \tag{5}$$

The second term on the LHS of Equation 5 modifies the frequency of oscillation of the system slightly, but is small for the cases presented here and can be neglected. Now, the pitch rate, $\dot{\theta}$, is be expressed in terms of $\dot{\alpha}$ and $\dot{\gamma}$. The first term on the RHS of Equation 5 becomes

$$C_{m_q} \frac{\dot{\theta} d}{2V} = C_{m_q} \left(\frac{\dot{\alpha} d}{2V} + \frac{\rho S d C_L}{4m} \right) \tag{6}$$

The $\dot{\gamma}$ term in Equation 6 is small compared to the $\dot{\alpha}$ term and may be neglected as well. Equation 5 then becomes

$$\ddot{\alpha} - \frac{\rho V S}{2m} \left(-C_{L_\alpha} + \frac{m d^2}{2I} \left(C_{m_q} + C_{m_{\dot{\alpha}}} \right) \right) \dot{\alpha} - \frac{\rho V^2 S d}{2I} C_{m_\alpha} \alpha = 0 \tag{7}$$

This equation is the starting point for the analysis of several test techniques. Each of the techniques impose further conditions that change the form of this equation. Three cases will be considered in this analysis. If the density and all aerodynamic coefficients are held constant, Equation 7 can be solved analytically for each case. The first case is a free-to-oscillate wind tunnel setup, where the model sees a constant velocity and is free to rotate only. The second case is also a wind tunnel case, where the model sees a constant velocity, but is free to

move normal to the freestream velocity vector due to lift in addition to being free to oscillate. For the third case, the model is permitted to decelerate due to drag and is still free to oscillate and heave normal to the freestream velocity vector.

4.0 CONSTANT COEFFICIENT ANALYTIC SOLUTIONS

This section will present analytic solutions to the three boundary condition cases just described in Section 3. It will be shown that these different boundary conditions affect the functional form of the solution to Equation 7. For each of these cases a set of common mass properties and initial flow conditions was used. For the constant velocity cases, the conditions remain constant. For the decelerating case, the model decelerates to a final condition. For each case, plots of oscillation histories for several constant pitch damping values are presented. The time-of-flight for the decelerating case was used as the time interval for all plots. Table 1 lists the mass properties and flow conditions used in the following sections. The initial and final times listed in Table 1 are along a timeline which assumes infinite initial velocity. This timeline allows some equation simplification required to obtain an analytical solution for the decelerating case. In all plots below, the timeline is shifted so that the simulated oscillations begin at $t_i = 0.0$.

Table 1: Example Test Parameters

Boundary Conditions		Range/Model Properties		Aerodynamics	
V_i	$858\ m/s$	m	$0.584\ kg$	C_{m_α}	$-0.09\ rad^{-1}$
V_f	$858\ m/s\ (\dot{V}=0),\ 343\ m/s\ (\dot{V}<0)$	I	$1.55 \cdot 10^{-4}\ kg \cdot m^2$	$C_D = C_A$	1.58
α_o	5°	d	$0.07\ m$	C_{L_α}	-1.58
$\dot{\alpha}_o$	$0\ rad/s$	S	$0.00385\ m^2$	$C_{m_q} + C_{m_{\dot{\alpha}}}$	$+0.15, 0, -0.171, -0.342$
t_1	$0.186\ s\ \ (t_i = 0.0\ s)$	ρ	$1.20\ kg/m^3$	C_N	0.0
t_2	$0.466\ s\ \ (t_f = 0.28\ s)$				

4.1 Case 1 : Constant Velocity, Free-to-Oscillate, No-Heave

For this case, Equation 7 must be simplified slightly. As the oscillation center is fixed relative to the freestream flow, there is no change in flight path angle due to the lift generated as the model oscillates, $\dot{\gamma} = 0$. Therefore the C_{L_α}term, really an expression for $\ddot{\gamma}$ substituted from the time derivative of Equation 2 drops out. This simplifies Equation 7 to

$$\ddot{\alpha} - \frac{\rho V_\infty S d^2}{4I}\left(C_{m_q} + C_{m_{\dot{\alpha}}}\right)\dot{\alpha} - \frac{\rho V_\infty^2 S d}{2I} C_{m_\alpha}\alpha = 0 \tag{8}$$

As all coefficients are constant, this equation is a simple harmonic oscillator with damping, having the classic solution

$$\alpha = A e^{\xi_1 t}\cos(\omega t + \delta) \tag{9}$$

where

$$\xi_1 = \frac{\rho V S d^2}{8I}(C_{m_q} + C_{m_{\dot{\alpha}}}) \tag{10}$$

and

$$\omega = \sqrt{-\frac{\rho V^2 S d}{2I} C_{m_\alpha}} \tag{11}$$

Figure 5 shows a plot of Equation 9 for several values of $C_{m_q} + C_{m_{\dot{\alpha}}}$. For this case, understanding the oscillations is very straight forward. Positive values for $C_{m_q} + C_{m_{\dot{\alpha}}}$ cause oscillation amplitude growth, while negative values damp down any oscillations. These test conditions are ideal for isolating and identifying dynamic damping characteristics inherent to the geometry of the vehicle. The dynamic stability is the only term affecting the oscillation amplitude growth.

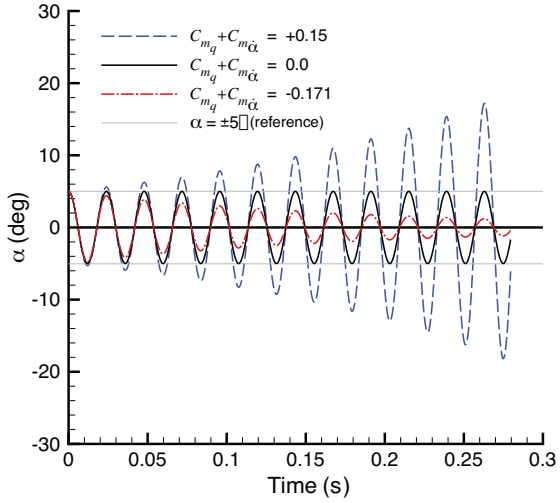

Figure 5: Oscillation amplitude history for different damping values, constant velocity, no heaving motion.

4.2 Case 2: Constant Velocity, Free-to-Oscillate, Free-to-heave

Here the body is held at constant velocity, but also allowed to move normal to the velocity vector due to the lift generated as the model oscillates rotationally. This extra degree of freedom results in transverse oscillatory motion which induces changes to the angle-of-attack history. This setup is described correctly by Equation 7. Again we have constant coefficients, so the solution is of the same form,

$$\alpha = Ae^{\xi_2 t}\cos(\omega t + \delta) \tag{12}$$

However, C_{L_α} modifies the damping term as

$$\xi_2 = \frac{\rho V S}{4m}\left(-C_{L_\alpha} + \frac{md^2}{2I}(C_{m_q} + C_{m_{\dot{\alpha}}})\right) = \xi_1 - \frac{\rho V S}{4m} C_{L_\alpha} \tag{13}$$

Here, we can make one more substitution for blunt bodies at small angles of attack. For small to moderate angles of attack ($\alpha \lesssim 30^\circ$), normal forces acting on a blunt body are much smaller than axial forces ($C_N \ll C_A$). The lift and drag equations in terms of the normal and axial forces acting on a blunt body can then be simplified to yield

$$\left.\begin{array}{c} C_D = C_A \cos\alpha - C_N \sin\alpha \approx C_A \cos\alpha \approx C_A \\ C_L = C_N \cos\alpha - C_A \sin\alpha \approx -C_A \alpha \\ C_{L_\alpha} \approx -C_A \end{array}\right\} \tag{14}$$

Substituting into Equation 13, the damping term for the constant velocity, free-to-heave case is

$$\xi_2 = \xi_1 + \frac{\rho V S C_A}{4m} \tag{15}$$

Figure 6 shows a plot of Equation 12 for several values of $C_{m_q} + C_{m_{\dot{\alpha}}}$. As the equations suggest, for no amplitude growth, the dynamic damping coefficient must be negative to balance the undamping due to lift.

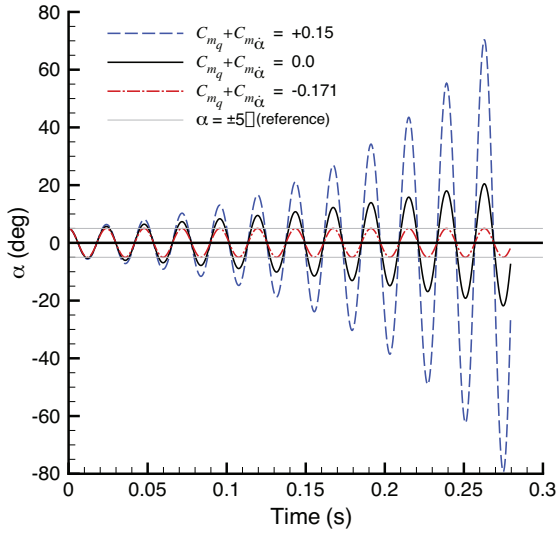

Figure 6: Oscillation amplitude history for different damping values, constant velocity with heaving motion due to lift.

The damping term indicates that allowing the body to move transverse to the oncoming flow results in a more undamped system for blunt bodies. It is important to note that this is fairly specific to blunt bodies only. The lift generated by blunt bodies is almost entirely due to the pointing of the axial force vector. Therefore, to generate an upward lift, the body nose must be at a negative angle-of-attack. This is opposite to winged aircraft and results in the increased undamping of the system. As a blunt body rotates, nose-down, lift causes the body to move up. This upward velocity causes an induced increment to angle of attack. In contrast, a winged vehicle typically pitches up to increase lift. The upward rotation results in an upward motion, inducing a decrease in the angle-of-attack seen by the vehicle. The effects of static aerodynamics on damping will be discussed again in Section 5 when the energy equation is applied to this system.

4.3 Case 3: Decelerating, Free-to-Oscillate, Free-to-Heave

Now, the body is allowed to decelerate and again, the body is permitted to heave. This heaving degree-of-freedom has an effect similar to that seen in the previous constant velocity case. The no-heave decelerating case will not be shown, as it is not a common test setup. However, a ballistic range test is very closely approximated by Equation 7 if velocity is allowed to vary with time. For this case, velocity is permitted to decrease due to drag acting on the vehicle and lift is the only force changing the flight path angle. Again, this is valid for small

oscillations. The approximations made in Equation 14 hold. Schoenenberger, Queen and Litton [13] developed the following solution for this decelerating case. The results presented here are explained in more detail in that work. For a constant drag coefficient (invariant with small oscillations), the deceleration of a body can be expressed as

$$V = \frac{2m}{\rho S C_A t} \tag{16}$$

Substituting this expression into Equation 7 and some rearranging yields

$$t^2\ddot{\alpha} - \left(1 + \frac{md^2}{2I}\frac{\left(C_{m_q} + C_{m_{\dot{\alpha}}}\right)}{C_A}\right) t\dot{\alpha} - \frac{2m^2 dC_{m_\alpha}}{\rho S I C_A^2}\alpha = 0 \tag{17}$$

Note, in Equation 16, velocity is infinite at time, $t = 0$. Solving Equation 17 must be done on a timeline that starts at infinite velocity. This is handled by solving Equation 16 for an initial time, $t_i > 0$, that corresponds to the desired initial velocity.

$$t_i = \frac{\rho V_i S C_A}{2m} \tag{18}$$

While awkward, the simplified version of the deceleration equation yields a differential equation with an analytic solution. Equation 17 is the Euler-Cauchy equation[14] and has the following solution

$$\alpha = At^{\mu}\cos(\nu \ln t + \delta) \tag{19}$$

Where A is a constant determined by the angle-of-attack oscillation amplitude at the boundary conditions and the constant δ is a phase lag determined from the boundary conditions. Oscillation amplitude grows with time, raised the the power, μ. The coefficient ,μ, is

$$\mu = \frac{md^2\left(C_{m_q} + C_{m_{\dot{\alpha}}}\right)}{4IC_A} + 1 \tag{20}$$

For a body with $C_{m_q} + C_{m_{\dot{\alpha}}} = 0$, oscillation amplitudes will grow in direct proportion to time ($\alpha_0 \propto t$) while the velocity decreases as $1/t$. As with the constant velocity case, the change in flight path angle due to the lift curve slope, $-C_{L_\alpha}$, results in an oscillation amplitude growth even without a contribution from the dynamic stability coefficient. However, the functional form of the oscillation growth has changed. The coefficient, ν, is

$$\nu = \sqrt{\mu^2 - \frac{2mdC_{m_\alpha}}{\rho S I C_A^2}} \approx \sqrt{-\frac{2m^2 dC_{m_\alpha}}{\rho S I C_A^2}} \tag{21}$$

As with the constant velocity version, for the aerodynamics of typical blunt bodies, the damping coefficient in Equation 17 is very small compared to the static stability coefficient.

Figure 7 shows a plot of Equation 19 for several values of $C_{m_q} + C_{m_{\dot{\alpha}}}$. As the equations suggest, for no amplitude growth, the dynamic damping must be negative to counteract the undamping due to lift and natural growth due to decreasing dynamic pressure. The value of $C_{m_q} + C_{m_{\dot{\alpha}}}$ required for no amplitude growth is exactly twice that for the constant velocity, free-to-heave case.

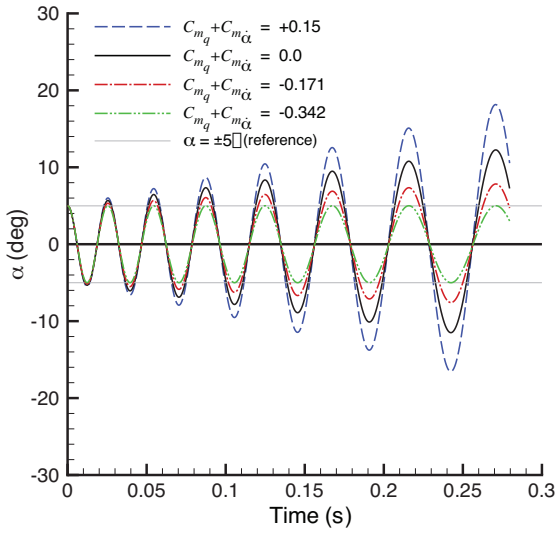

Figure 7: Oscillation amplitude history for different damping values, decelerating with heaving motion due to lift.

5.0 ENERGY EQUATION ANALYSIS

Here we will look at the energy of an oscillating system with no damping for the three different cases that occur in wind tunnel and ballistic range testing. This use of the energy equation is useful in highlighting the mechanisms that drive the oscillation growth or decay for different flight or test conditions. Time variation of energy will be derived for each case. The moment equation will help simplify the energy equation and show the system to be either conservative or not depending on the imposed flight conditions. The evaluation of each system will show how the dynamic stability and static aerodynamics contribute to the oscillatory energy. Later, an approach to find the effective damping for blunt bodies with nonlinear dynamic stability characteristics will be applied with this energy-equation analysis to predict equilibrium oscillations and constant energy oscillatory behavior.

In the inertial frame, the equation describing the oscillation energy of a free flying body is the sum of the kinetic and potential oscillatory energy:

$$K = \frac{1}{2} I\dot{\theta}^2 - \frac{1}{4}\rho V^2 SdC_{m_\alpha}\alpha^2 \tag{22}$$

The rate of change of this energy is then

$$\frac{dK}{dt} = I\ddot{\theta}\dot{\theta} - \frac{1}{2}\rho V^2 SdC_{m_\alpha}\alpha\dot{\alpha} - \frac{1}{2}\rho V SdC_{m_\alpha}\alpha^2\dot{V} \tag{23}$$

Now, the moment equation, with dynamic damping is

$$I\ddot{\theta} - \frac{1}{2}\rho V^2 Sd\left((C_{m_q} + C_{m_{\dot\alpha}})\frac{\dot{\alpha}d}{2V} + C_{m_\alpha}\alpha\right) = 0 \tag{24}$$

Multiplying the moment equation by $\dot{\theta}$ and expanding yields

$$I\ddot{\theta}\dot{\theta} = \frac{1}{2}\rho V^2 Sd\left((C_{m_q} + C_{m_{\dot\alpha}})\frac{(\dot{\alpha}^2 + \dot{\alpha}\dot{\gamma})d}{2V} + C_{m_\alpha}\alpha(\dot{\alpha} + \dot{\gamma})\right) \tag{25}$$

Substituting Equation 25 into Equation 23 yields

$$\frac{dK}{dt} = \frac{1}{2}\rho V^2 Sd\left((C_{m_q} + C_{m_{\dot\alpha}})\frac{(\dot\alpha^2 + \dot\alpha\dot\gamma)d}{2V}\right) + \frac{1}{2}\rho V^2 SdC_{m_\alpha}\alpha\dot\gamma - \frac{1}{2}\rho VSdC_{m_\alpha}\alpha^2\dot V \tag{26}$$

From the planar equations of motion we have

$$\dot\gamma = \frac{\rho VSC_L}{2m} \approx -\frac{\rho VSC_A}{2m}\alpha \tag{27}$$

and for a decelerating body

$$\dot V = -\frac{\rho V^2 SC_A}{2m} = \dot\gamma\frac{V}{\alpha} \tag{28}$$

For a constant velocity body the change in velocity is of course, zero

$$\dot V = 0 \tag{29}$$

Equations 26-29 provide the tools needed to understand at all three blunt body oscillation scenarios.

Constant Velocity, No-Heave

For a constant velocity case that is not allowed to heave we have

$$\dot V = 0, \;\; \dot\gamma = 0 \tag{30}$$

Equation 26 simplifies to

$$\frac{dK}{dt} = \frac{1}{4}\rho VSd^2(C_{m_q} + C_{m_{\dot\alpha}})\dot\alpha^2 \tag{31}$$

Energy enters the system only by the dynamic damping term. Integrating the change in energy over an entire cycle for this case yields

$$K_f = \frac{1}{4}\rho VSd^2\int_0^{\frac{2\pi}{\omega}}\left(C_{m_q} + C_{m_{\dot\alpha}}\right)\dot\alpha^2 dt + K_i \tag{32}$$

For $C_{m_q} + C_{m_{\dot\alpha}} = 0$, no energy is entering the system and K in Equation 32 is trivially equal to the initial energy of the system. Later, nonlinear pitch damping curves will be evaluated using this equation to find amplitudes of constant oscillatory energy.

Constant Velocity, Free-to-Heave, No Dynamic Damping

This case approximates a terminal velocity drop test, or vertical wind tunnel test, where drag and gravity's pull are in equilibrium, resulting in constant freestream velocity, yet still permitting motions normal to the oncoming flow. In practice, there may be coupling of the oscillatory motion and descent rate as the small angle approximations may be violated. This coupling is neglected here.

By allowing the model to change flight path angle due to lift (heave) at constant velocity, the problem becomes slightly more complicated. First, consider the case with no dynamic damping. In this case Equation 26 becomes

$$\frac{dK}{dt} = \frac{1}{2}\rho V^2 S d C_{m_\alpha} \alpha \dot{\gamma} = \frac{1}{2}\rho V^2 S d C_{m_\alpha} \alpha^2 \frac{\rho S V}{2m} C_{L_\alpha} \tag{33}$$

Even with no dynamic damping, rotational energy enters the system. To keep the model from decelerating, a sting or some other force must balance the drag force (approximately equal to the axial force for small oscillations). When the model oscillates, the lift generated by the body takes energy from the oncoming flow and converts it to oscillatory energy. Note that for blunt bodies, the lift curve slope is negative, so the change in energy is positive For a winged vehicle, the lift curve slope is typically positive, which results in the removal of oscillatory energy from the system. The static lift characteristics of blunt bodies, driven by the pointing of the axial force vector, results in an undamped bias to their dynamic stability. The steeper the lift curve slope, the greater this bias becomes.

The amount of energy that goes into the system is proportional to the dynamic pressure of the flow and the ratio of the approaching mass flux to the model mass. So, a model with a high density will see less transverse accelerations and therefore convert less of the energy in the freestream flow to oscillatory energy than a lower density body. The pitching moment slope and axial force coefficient also determine how efficiently the geometry of a particular body converts the freestream flow energy into oscillations.

Constant Velocity, Free-to-Heave, with Dynamic Damping

Now, the case with dynamic damping is considered. In this case, the $\dot{V}$ term in equation 26 is the only one that drops out immediately. Dropping the $\dot{V}$ term and rearranging we have

$$\frac{dK}{dt} = \frac{1}{2}\rho V^2 S d \left(C_{m_\alpha} \alpha + \left(C_{m_q} + C_{m_{\dot{\alpha}}} \right) \frac{\dot{\alpha} d}{2V} \right) \dot{\gamma} + \frac{1}{2}\rho V^2 S d \left(C_{m_q} + C_{m_{\dot{\alpha}}} \right) \frac{\dot{\alpha}^2 d}{2V} \tag{34}$$

Substituting the expression for $\dot{\gamma}$, Equation 2, into Equation 34 and again rearranging yields

$$\frac{dK}{dt} = \frac{\rho V S I}{2m} \left(\frac{\rho V^2 S d}{2I} C_{m_\alpha} C_{L_\alpha} \alpha^2 + \frac{m d^2}{2I} \left(C_{m_q} + C_{m_{\dot{\alpha}}} \right) \dot{\alpha}^2 \right) + \left(C_{m_q} + C_{m_{\dot{\alpha}}} \right) \frac{1}{2}\rho V^2 S d \frac{\rho S d}{4m} C_{L_\alpha} \alpha \dot{\alpha} \tag{35}$$

For a constant velocity limit cycle, where the damping is not a large component of the total pitching moment, the angle-of-attack history can be represented as a sinusoid.

$$\alpha = A \cos(\omega t) \tag{36}$$

$$\dot{\alpha} = -A\omega \sin(\omega t) \tag{37}$$

Here, the frequency of oscillation, ω, from the static stability term in the moment equation, given in Equation 11 is used. Substituting Equation 11 into Equation 35 yields

$$\frac{dK}{dt} = \frac{\rho V S I}{2m} \left(-C_{L_\alpha} \omega^2 \alpha^2 + \frac{m d^2}{2I} \left(C_{m_q} + C_{m_{\dot{\alpha}}} \right) \dot{\alpha}^2 \right) + \left(C_{m_q} + C_{m_{\dot{\alpha}}} \right) \frac{1}{2}\rho V^2 S d \frac{\rho S d}{4m} C_{L_\alpha} \alpha \dot{\alpha} \tag{38}$$

Now an expression for the total rotational energy entering the system (the integral of Equation 38) may be set to zero to find the damping required for a limit cycle. The integral of the energy rate must be integrated over a complete cycle. With that constraint, and Equations 36 and 37 for α and $\dot{\alpha}$, the following relation holds,

$$\int_0^{\frac{2\pi}{\omega}} \omega^2 \alpha^2 dt = \int_0^{\frac{2\pi}{\omega}} \dot{\alpha}^2 dt \tag{39}$$

After substituting Equation 39 into Equation 38, the integral is taken to obtain the total oscillatory energy added to a constant velocity, free-to-heave system with damping. For no oscillation amplitude growth for this constant velocity case, the net energy added must be zero.

$$K_f = \frac{\rho V S I}{2m} \int_0^{\frac{2\pi}{\omega}} \left(-C_{L_\alpha} + \frac{md^2}{2I} \left(C_{m_q} + C_{m_{\dot{\alpha}}} \right) \right) \dot{\alpha}^2 dt + K_i = 0 \tag{40}$$

Note that the integral of the $\alpha\dot{\alpha}$ term in Equation 38 disappears when integrated over a complete cycle. Recalling Equation 7, this is exactly the integral of the moment equation, expressed in terms of angle-of-attack only, multiplied by the rate of change of angle-of-attack, $\dot{\alpha}$. Thus, it has been shown that for a constant velocity system, the dynamic stability of the blunt body must be negative to balance the energy added due to heaving motions, induced ultimately by the force required to maintain the constant velocity. The particular static aerodynamics of the vehicle determine how effectively the drag force is converted to oscillations. In that sense the amplitude of a limit cycle is driven by both the dynamic stability characteristics and the static aerodynamics.

Decelerating, Free-to-Heave

The decelerating case is the last case for consideration. Substituting Equation 16 into 2 and 1 yields

$$\dot{\gamma} = -\frac{\alpha}{t} \tag{41}$$

$$\dot{V} = \dot{\gamma}\frac{V}{\alpha} = -\frac{V}{t} \tag{42}$$

These expressions can then be substituted to simplify Equation 26

$$\frac{dK}{dt} = \frac{md^2}{2C_A t} \left((C_{m_q} + C_{m_{\dot{\alpha}}})(\dot{\alpha}^2 - \frac{\dot{\alpha}\alpha}{t}) \right) - \frac{1}{2}\rho V^2 S d C_{m_\alpha} \frac{\alpha^2}{t} + \frac{1}{2}\rho V^2 S d C_{m_\alpha} \frac{\alpha^2}{t} \tag{43}$$

The last two terms obviously cancel leaving only a dynamic damping term to add or remove energy from the oscillatory system. The trivial case, $C_{m_q} + C_{m_{\dot{\alpha}}} = 0$, results in a conservative system, $\frac{dK}{dt} = 0$, even though the analytical solution shows that the oscillation amplitude grows linearly with time (Equation 19). The energy entering the system due to the body lifting is negated exactly by the decrease in dynamic pressure as the body decelerates. The $\frac{\dot{\alpha}\alpha}{t}$ term in Equation 43 modifies the rate at which dynamic damping adds or removes oscillatory energy in the system. When integrated over a full cycle this term is small and may be neglected. However, for this decelerating case, both oscillation amplitude and velocity are changing with time for a constant energy system. Nonlinear pitch damping curves typically vary significantly with both amplitude and Mach number, so it is difficult to use the mean value theorem to find an average damping coefficient that resulted in no net energy over more than a few oscillation cycles.

6.0 PITCH DAMPING CHARACTERISTICS OF BLUNT BODIES

To understand limit cycles for each of the cases presented in Sections 4 and 5 it is important to discuss the dynamic damping coefficients, typical of blunt bodies. In the supersonic regime, the pitch and yaw damping of blunt bodies can be very nonlinear. Some typical pitch damping curves are presented here and the mean value theorem is applied to average the effect of the dynamic damping coefficients over a full oscillation cycle.

6.1 Typical Pitch Damping Characteristics

Figure 8 shows several pitch damping curves extracted from ballistic range tests of the Mars Exploration Rover (MER) entry Capsule[15]. The $C_{m_q} + C_{m_{\dot{\alpha}}}$ values are positive at small angles of attack, crossing zero and becoming negative at large angles. This results in negative damping at small angles which tends to increase oscillation amplitudes until the undamped region is balanced by the positive damping at large angles, thus reaching a limit cycle. Data for several Mach numbers are shown. As the capsule decelerates the undamped region becomes more unstable and extends to greater angles-of-attack. The features in Figure 8 are typical of many blunt bodies. The analytic solutions developed earlier can not be applied directly to assess or compare the dynamic characteristics of blunt bodies with such nonlinear pitch damping curves. The mean value theorem will now be used to calculate constant-value equivalents to these curves as a function of oscillation amplitude. The dynamic damping curves will then be cast in a form suitable for interpretation using the analytic solutions.

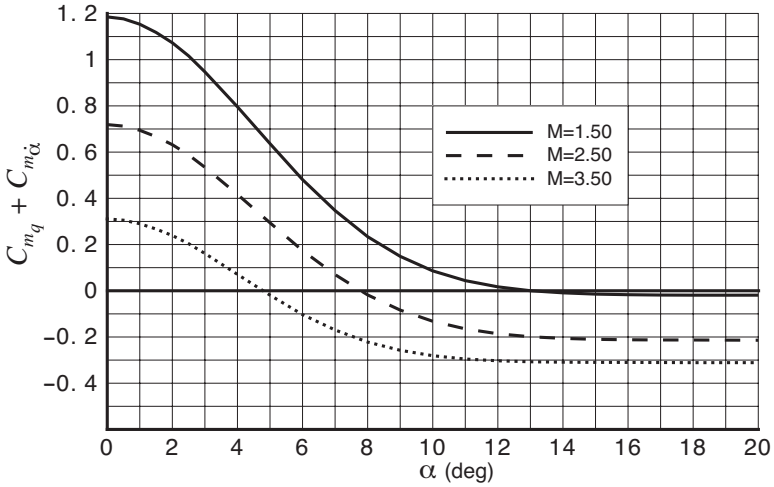

Figure 8: Example pitch damping data from Mars Exploration Rover ballistic range data, $x_{cg}/D = 0.30$.

6.2 Mean Value Theorem Averaging

For the nonconservative systems described in Section 5, the rate at which energy is added or removed is a function of the dynamic stability, multiplied by the square of the angular rate. To evaluate the nonlinear damping properties of blunt bodies, it is useful to integrate the dynamic damping effects over an entire cycle. The mean value theorem allows a very nonlinear curve to be replaced with a constant value for oscillations of constant amplitude (i.e. a constant velocity limit cycle) and can be applied for a few oscillations where the amplitude is not growing or decaying significantly. This averaging can find the amplitude where dynamic stability is effectively zero or can find the damping required to balance the lift-curve slope and deceleration effects.

Redd et al[16] showed that system damping characterized by a function of instantaneous angle-of-attack can also be represented as a mean value that varies as a function of oscillation amplitude. Redd made the reasonable assumption that the energy entering or leaving the system per cycle is the same whether damping is a function of instantaneous angle-of-attack or oscillation amplitude. This enabled the use of the mean value theorem to average any nonlinear damping function with angle of attack to obtain a constant, mean value. This mean value can be substituted for the nonlinear curve and the system will act the same.

$$\int_0^T f(\alpha)\dot{\alpha}^2 dt = f(\alpha_o)\int_0^T \dot{\alpha}^2 dt \tag{44}$$

$$f(\alpha_o) = \frac{\int_0^T f(\alpha)\dot{\alpha}^2 dt}{\int_0^T \dot{\alpha}^2 dt} \tag{45}$$

This approach can be applied to any of the energy rate equations presented in Section 5. Integrating the power over a full cycle can be used to find the constant-amplitude equilibrium point or find an amplitude where no net energy is entering the system (not necessarily the same conditions) for a system with nonlinear damping.

Recall the constant velocity, no-heave and free-to-heave energy rate equations (Equations 31 and 40). By casting these power equations in the form of Equation 45, the effective damping as a function of oscillation amplitude may be determined.

For the constant velocity, no-heave case the effective damping is

$$\overline{C_{m_q}} = \frac{\int_0^{\frac{2\pi}{\omega}} \left(C_{m_q} + C_{m_{\dot{\alpha}}}\right)\dot{\alpha}^2 dt}{\int_0^{\frac{2\pi}{\omega}} \dot{\alpha}^2 dt} \tag{46}$$

Likewise the constant velocity, free-to-heave effective damping is

$$\overline{-C_{L_\alpha} + C_{m_q}} = \frac{\int_0^{\frac{2\pi}{\omega}} \left(-\frac{2I}{md^2}C_{L_\alpha} + \left(C_{m_q} + C_{m_{\dot{\alpha}}}\right)\right)\dot{\alpha}^2 dt}{\int_0^{\frac{2\pi}{\omega}} \dot{\alpha}^2 dt} \tag{47}$$

Where $\overline{C_{m_q}}$ and $\overline{-C_{L_\alpha} + C_{m_q}}$ are shorthand terms used to represent the mean effective damping determined by evaluating the RHS of equations 46 and 47 for a particular oscillation amplitude, α_0. To analytically solve these expressions, the lift curve slope and nonlinear pitch damping must be modeled as a function of angle of attack (itself a periodic function of time) that yields an analytically solvable equation. Otherwise, this expression must be evaluated numerically. For small amplitude growth over a single cycle, this relation can be used to assess the effective damping away from the limit cycle amplitude. The oscillation amplitude for which Equation 47 is equal to zero is where the dynamic damping balances the C_{L_α} contribution, satisfying Equation 40.

For the example used throughout this paper, the lift curve slope is assumed constant. In this case, Equation 47 can be simplified even further

$$\overline{-C_{L_\alpha} + C_{m_q}} = -\frac{2I}{md^2}C_{L_\alpha} + \overline{C_{m_q}} \tag{48}$$

For a given oscillation amplitude, the effective damping for a constant velocity, free-to-heave system is identical to the damping of the constant velocity, no-heave system, offset by a constant factor. For a blunt body with nonlinear dynamics like those described in Section 6.1, and all other conditions equal, a blunt body that is free-to-heave will reach oscillatory equilibrium at a larger amplitude than for a system, that is constrained against translation from lift.

7.0 LIMIT CYCLE DISCUSSION

Discussions about oscillation amplitudes and energy to this point have been careful to avoid the term "limit cycle". This is because for some of the cases presented, a constant amplitude oscillation does not correspond to a constant energy system. Conversely, some constant-energy systems grow in amplitude. Looking at the effective damping equations derived in the previous section, both were derived from the energy equation. Evaluating Equations 46 or 47 to find where $\overline{C_{m_q}}$ or $\overline{-C_{L_\alpha} + C_{m_q}}$ is zero, finds the point where oscillation amplitude is constant and there is no net energy entering or leaving the system. However, this does not hold for the decelerating case. Applying mean value theorem to the decelerating, free-to-heave energy equation (Equation 43) yields

$$\overline{C_{m_{q,decel}}} = \frac{\int_{t_1=e^{-\frac{\delta}{\nu}}}^{t_2=e^{\frac{2\pi-\delta}{\nu}}} \left(C_{m_q} + C_{m_{\dot{\alpha}}}\right)\left(\frac{\dot{\alpha}^2}{t} - \frac{\dot{\alpha}\alpha}{t^2}\right) dt}{\int_{t_1=e^{-\frac{\delta}{\nu}}}^{t_2=e^{\frac{2\pi-\delta}{\nu}}} \left(\frac{\dot{\alpha}^2}{t} - \frac{\dot{\alpha}\alpha}{t^2}\right) dt} \tag{49}$$

Note that the limits of integration are those for a full cycle of the analytic solution of the Euler-Cauchy equation, derived for the decelerating case (Equation 19). Evaluating this expression to find an amplitude where $\overline{C_{m_{q,decel}}}$ is zero does find the amplitude where no net energy is entering the oscillatory system. However, as was shown in the analytical solution for the decelerating case, $C_{m_q} = 0$ does not correspond to a constant amplitude oscillation. The dynamic pressure is dropping, decreasing the "spring stiffness" of the system and oscillation amplitude grows linearly. The exponent, μ, in Equation 19, can be used to predict the constant oscillation amplitude for decelerating, free-to-heave system with nonlinear dynamic damping. The mean value theorem allows an average value to replace a nonlinear function for a given oscillation amplitude. The effective damping that satisfies $\mu = 0$ should result in a constant oscillation amplitude. This is effectively finding the damping that will result in the net energy loss required to achieve a constant amplitude oscillation. This is analogous to the constant offset difference between the free-to-heave and no-heave constant velocity cases. Setting μ to zero in Equation 20 and rearranging yields

$$C_{m_q} + C_{m_{\dot{\alpha}}}\Big|_{\alpha_0=constant} = -\frac{4IC_A}{md^2} \approx \frac{4I}{md^2} C_{L_\alpha} \tag{50}$$

This is twice the factor by which the two constant velocity cases differed. To be at oscillation amplitude equilibrium, a decelerating blunt body that is free to heave must have positive dynamic damping ($\overline{C_{m_q}} < 0$), twice that needed for the constant velocity, free-to-heave case. This gets at the role of dynamic damping and its relation to oscillation amplitude and energy under different test conditions. For all of this analysis, the oscillatory energy is the only energy of the system being considered. The point-mass kinetic energy of the system is also changing, often to a much greater extent than the oscillatory energy. Take for example, the constant velocity, free-to-heave case. Those conditions closely approximate a blunt body falling at terminal velocity. In that case, the loss of potential energy is essentially balanced by the work done on the body by aerodynamic drag. The small lift force generated as the model decelerates "bleeds" a small amount of the kinetic energy into the oscillatory system. This amount is so small, so as not to affect the terminal velocity significantly, but large enough to have a very noticeable effect on the the oscillatory behavior of the system. With no dynamic damping or nonlinear aerodynamics countering the energy being added to the system from lift, a blunt body at terminal velocity will eventually flip over. For a decelerating case, the point-mass kinetic energy of the

system is decreasing as aerodynamic forces decelerate the body. This deceleration reduces dynamic pressure and causes oscillations to grow in amplitude and drop in frequency. Even without the energy cross-talk due to lift, a decelerating case must have dynamic damping to keep oscillations from growing in amplitude.

7.1 Example Case

Pitch Damping Model

To illustrate the application of the mean value theorem in predicting oscillation equilibrium, a nonlinear pitch damping curve will be evaluated. This curve replaces the constant values in the original example first described in Section 4. For these cases the time-of-flight is extended to one second to show the convergence towards oscillation equilibrium. All other conditions described in Table 1 are unchanged. Figure 9a shows the example nonlinear pitch damping curve used for this analysis. The curve is parabolic at small angles, switching to a constant, negative value at all large angles of attack. While made-up, it is representative of pitch damping curves seen in blunt body dynamic testing [11]. Figure 9b shows the effective damping for a range of oscillation amplitudes determined by the application of Equations 46, and 49 to the nonlinear damping curve. $C_{m_q}(\alpha)$. Note that integrating over complete constant velocity and decelerating cycles produce almost identical effective damping curves. The points on the plot are the predicted equilibrium oscillation amplitudes for the three cases. Also noted is the amplitude at which the decelerating case sees no net energy addition. As shown in Section 4, the oscillation amplitude for this case is still increasing. Figure 9b suggests that the amplitude growth-rate will decrease as the capsule passes through this constant-energy amplitude. The effective damping coefficient, $\overline{C_{m_q}}$, for the decelerating case, becomes negative as the body spends more time in the dynamically damped region of the $C_{m_q} + C_{m_{\dot{\alpha}}}$ curve.

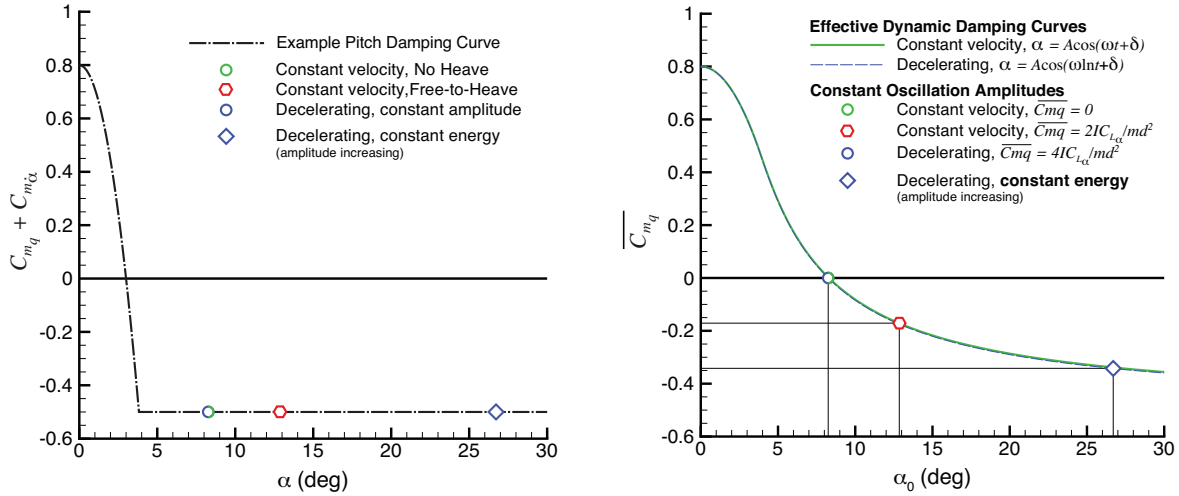

(a) Damping as function of instantaneous angle of attack

(b) Damping as function of amplitude

Figure 9: Pitch damping curve and integrated effective damping, noting constant amplitude and energy points for three cases.

Simulations

To demonstrate the effect of the example nonlinear damping, some simulations of the three test conditions are presented. For the two constant velocity cases, the model is placed at initial angles above and below the

equilibrium amplitudes predicted in Figure 9. For the decelerating case, initial angles above, below and at the predicted equilibrium oscillation amplitude are used.

Figure 10 shows simulations of the constant velocity cases at Mach = 2.5. Initial angles-of-attack are 20° and 2° degrees for both. All simulations reach the predicted oscillation amplitude for the particular boundary conditions. Note that the case where lift contributes to the oscillatory energy takes longer to reach equilibrium. Equation 48 shows that the lifting term effectively shifts the dynamic stability curve by a positive bias. This shift has two effects. First the positive region of the pitch damping curve is bigger, meaning the capsule will grow to a larger amplitude before reaching equilibrium (as shown). More energy enters the system at small angles. Second, the negative portion of the curve is shifted up, becoming less effective at damping oscillations toward equilibrium. For this particular example, if the lift curve slope were steep enough, the effective damping could be completely positive resulting in oscillation divergence.

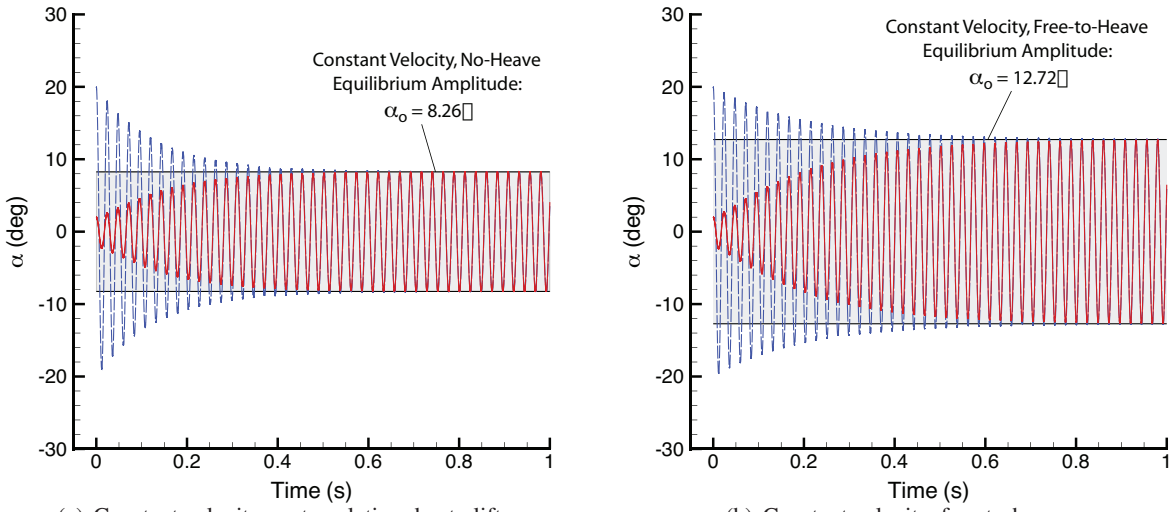

(a) Constant velocity, no translation due to lift

(b) Constant velocity, free-to-heave

Figure 10: Constant velocity oscillations approaching predicted equilibrium oscillations, $\alpha_i = 2°, 20°$.

Figure 11 shows simulations of the decelerating system. Note that the Mach number of the model as it decelerates drops from an initial value of Mach=2.5 down to approximately Mach=0.40. As was seen in the analytical solutions in Section 4, the frequency of oscillation decreases as the model slows down, but the amplitude converges towards an equilibrium amplitude consistent with the prediction in Figure 9. The shift in the effective damping due to lifting effects occurs in this case as in the constant velocity simulation. However, the decrease in dynamic pressure further reduces the damping of the system. This is supported by Equation 43 which shows the energy rate for this system to be decreasing with time. As the conditions shown here are representative of real ballistic range flight conditions, mass properties and aerodynamics, it is clear that direct observation of the steady-state amplitude can be difficult to achieve.

The low initial angle-of-attack case was started at the predicted constant energy amplitude (see Figure 9). This is the angle of attack where pitch damping does not add or subtract energy from the system ($dK/dt = 0$) and oscillations grow due to the drop in dynamic pressure only. The predicted amplitude for $\overline{C_{m_q}} = 0$ is plotted in Figure 11b. For approximately one cycle the simulation follows the constant energy prediction fairly closely. As the amplitude grows the negative portion of the nonlinear pitch damping curve contributes more to the overall damping and the oscillations grow less rapidly.

As dynamic pressure drops, the damping becomes less and less effective. Therefore, large displacements

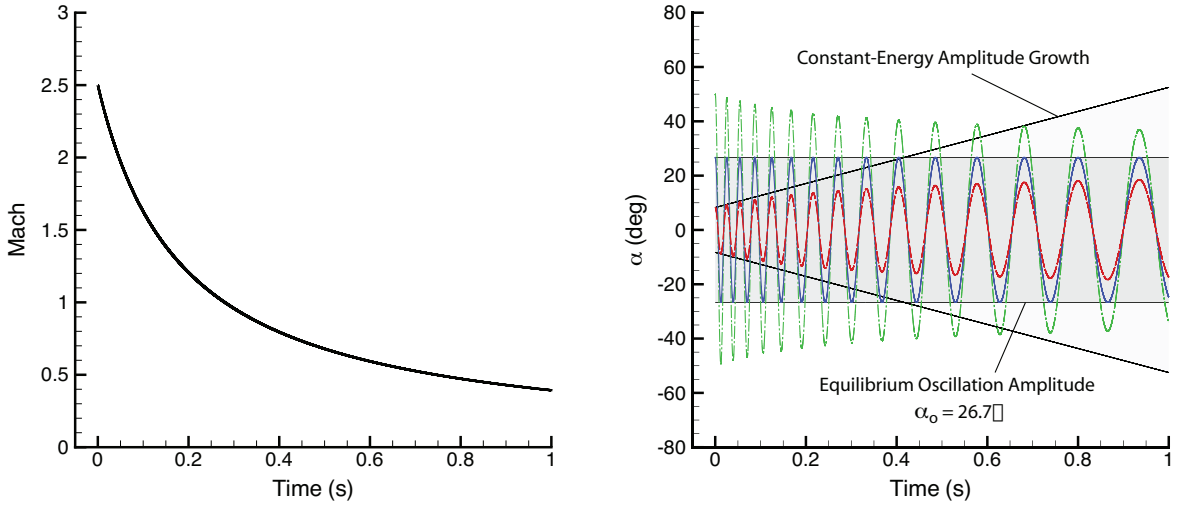

(a) Mach history (b) Decelerating, free-to-heave

Figure 11: Simulations of decelerating, free-to-heave system with predicted constant energy and equilibrium amplitude limits, $\alpha_i = 8.3,\ 26.7°$ and $50°$. Mach vs. time is shown for reference.

from the equilibrium amplitude take a long time to damp or grow to that amplitude. To verify the predicted equilibrium oscillation, a case starting at the predicted amplitude was run. As expected, the capsule remained at the initial amplitude. It is important to keep in mind that the oscillatory energy of this constant-amplitude system is continually decreasing with the drop in dynamic pressure.

8.0 CONCLUSIONS

This work has shown analytic solutions to three blunt-body oscillatory systems that are representative of test techniques frequently used to measure dynamic stability. Using the analytic solutions and the energy equation, the effects of the boundary conditions for each setup on the equilibrium energy behavior and equilibrium oscillation amplitude were determined. This should help the test engineer interpret different test results of a particular vehicle and better understand the effects a particular test technique has on blunt body oscillatory motions. One key feature of blunt body aerodynamics is that the lift curve slope is typically negative. This results in a natural undamping of the system when the body is free to translate due to lift. This is in contrast to a winged vehicle with a positive lift curve slope, which sees a natural positive damping for any disturbance from trim.

When the model is allowed to decelerate, the definition of “limit cycle” becomes somewhat cloudy. A decelerating system with no dynamic damping will grow in amplitude, yet that oscillatory energy of the system is constant. A damped decelerating system that reaches an equilibrium amplitude is losing oscillatory energy as the frequency of oscillation is dropping due to the drop in dynamic pressure. This paper has been careful to refer to either an oscillation equilibrium amplitude, or constant energy oscillation growth. A limit cycle seems to imply an equilibrium on oscillation amplitude, but should also reflect an energy balance. For the decelerating system these two conditions are not coincident. When interpreting test results it is good to look for regions where nonlinear dynamic damping is in equilibrium, while keeping in mind the test conditions and how they modify the dynamic behavior. This can be due to translation from lift as well as the change in dynamic pressure from deceleration.

Several effects were not addressed in this work. Density varies greatly along a planetary entry trajectory. This will modify the dynamic pressure differently than the constant density analysis shown here. Early along an entry profile, dynamic pressure is increasing due to density and freestream pressure rise, even though the capsule is decelerating. These effects should be considered in future work. Also, pitch damping and lift can vary significantly with Mach number. This complicates the analysis presented here. In practice it means that many more ballistic range or wind tunnel test conditions are required to fully determine the nonlinear pitch damping characteristics of blunt bodies.

There is currently no formal methodology for building ballistic range test matrices. There has historically been a lack of control of initial conditions, driven in part by sabot separation dynamics. In general a test engineer strives to obtain data of the test article oscillating about a number of different amplitudes, at different velocities, to anchor multi-fit 6-DoF simulation, solving for the aerodynamic coefficients. Future ballistic range testing might consider building test matrices to explicitly search for the equilibrium oscillation amplitude and constant energy amplitude growth behavior of the capsule. This would require greater control of initial conditions and more data per oscillation cycle than is typically gathered in spark-shadowgraph ranges. To find the amplitude of constant energy oscillation growth, high-speed movies or onboard telemetry would be required to measure the exact amplitude growth over a few cycles. Direct measurement of the oscillation amplitude is key for the equilibrium amplitude as well. Measuring free-flight data at a sufficient rate and with sufficient fidelity would be difficult, and many shots would be required to hunt for these characteristic features. However, designing tests to accurately measure amplitude growth, or for now, looking at available data with these features in mind might help to better define the functional forms of dynamic stability curves. The preceding work places new constraints on the functional form of damping derivatives. More accurate functional forms would greatly facilitate all parameter identification techniques for determining blunt body capsule damping.

REFERENCES

[1] Teramoto, S., Hiraki, K., and Fugii, K., "Numerical Analysis of Dynamic Stability of a Reentry Capsule at Transonic Speeds," *AIAA Journal*, Vol. 39, No. 4, April 2001, pp. 646–653.

[2] Murman, S. M. and Aftosmis, M. J., "Dynamic Analysis of Atmospheric-Entry Probes and Capsules," AIAA 2007–0074, January 2007.

[3] Chapman, G. T. and Yates, L. A., "Limit Cycle Analysis of Blunt Entry Vehicles," AIAA 99–1022, January 1999.

[4] Schueler, C. J., Ward, L. K., and Hodapp, A. E. J., "Techniques for Measurement of Dynamic Stability Derivatives in Ground Test Facilities," AGARDograph 121, 1967.

[5] Braslow, A. L., Harleth, G. W., and Cullen, Q. L., "A Rigidly Forced Oscillation System for Measuring Dynamic-Stability Parameters in Transonic and Supersonic Wind Tunnels," Tech. Rep. NASA TN D-1231, 1962.

[6] Moseley, William C.Jr.and Moore, R. H. J. and Hughes, J. E., "Stability Characteristics of the Apollo Command Module," Tech. Rep. NASA TN D-3890, 1967.

[7] "Cross Section of 20 FT Spin Tunnel," Image Number, EL-2001-00390, NASA Langley Research Center, 1953.

[8] "Mercury Capsule Model in Spin Tunnel," Image Number, EL-2000-00409, NASA Langley Research Center, 1959.

[9] Steinberg, S., Uselton, B., and Siemers, P., "Viking Configuration Pitch Damping Derivatives as Influenced by Support Interference and Test Technique at Transonic and Supersonic Speeds," AIAA 72–1012, September 1972.

[10] Cheatwood, F., Winchenbach, G., Hathaway, W., and Chapman, G., "Dynamic Stability Testing of the Genesis Sample Return Capsule," AIAA 2000–1009, January 2000.

[11] Winchenbach, G., Chapman, G., Hathaway, W., Ramsey, A., and Berner, C., "Dynamic Stability of Blunt Atmospheric Entry Configurations," *Journal of Spacecraft and Rockets*, Vol. 39, No. 1, 2002, pp. 49–55.

[12] Winchenbach, G. L., "Aerodynamic Testing in a Free-Flight Spark Range," Tech. Rep. WL-TR-1997-7006, Wright Laboratory, Armament Directorate, Weapon Flight Mechanics Division (WL/MNAV), Eglin AFB, FL, April 1997.

[13] Schoenenberger, M., Queen, E. M., and Litton, D., "Oscillation Amplitude Growth for a Decelerating Object with Constant Pitch Damping," AIAA 2006–6148, 2006.

[14] Kreyszig, E., *Advanced Engineering Mathematics*, John Wiley and Sons, Inc., New York, 1988.

[15] Schoenenberger, M., Hathaway, W., Yates, L., and Desai, P., "Ballistic Range Testing of the Mars Exploration Rover Entry Capsule," AIAA 2005–0055, January 2005.

[16] Redd, B., Olsen, D. M., and Barton, R. L., "Relationship Between the Aerodynamic Damping Derivatives Measured as a Function of Instantaneous Angular Displacement and the Aerodynamic Damping Derivatives Measured as a Function of Oscillation Amplitude," Tech. Rep. NASA TN D-2855, 1965.